AIP | Applied Physics Letters

# Switching phase separation mode by varying the hydrophobicity of polymer additives in solution-processed semiconducting small-molecule/polymer blends

Zhengran He, Dawen Li, Dale K. Hensley, Adam J. Rondinone, and Jihua Chen

Citation: Appl. Phys. Lett. **103**, 113301 (2013); doi: 10.1063/1.4820588
View online: http://dx.doi.org/10.1063/1.4820588
View Table of Contents: http://apl.aip.org/resource/1/APPLAB/v103/i11
Published by the AIP Publishing LLC.

## Additional information on Appl. Phys. Lett.

Journal Homepage: http://apl.aip.org/
Journal Information: http://apl.aip.org/about/about_the_journal
Top downloads: http://apl.aip.org/features/most_downloaded
Information for Authors: http://apl.aip.org/authors

ADVERTISEMENT

# Switching phase separation mode by varying the hydrophobicity of polymer additives in solution-processed semiconducting small-molecule/polymer blends

Zhengran He,[1] Dawen Li,[1,a)] Dale K. Hensley,[2] Adam J. Rondinone,[2] and Jihua Chen[2,a)]
[1]*Department of Electrical and Computer Engineering, Center for Materials for Information Technology, The University of Alabama, Tuscaloosa, Alabama 35487, USA*
[2]*Center for Nanophase Materials Sciences, Oak Ridge National Laboratory, Oak Ridge, Tennessee 37831, USA*

(Received 18 May 2013; accepted 22 August 2013; published online 10 September 2013)

Lateral and vertical phase separations play critical roles in the performance of the next-generation organic and hybrid electronic devices. A method is demonstrated here to switch between lateral and vertical phase separations in semiconducting 6,13-bis(triisopropylsilylethynyl) pentacene (TIPSE pentacene)/polymer blend films by simply varying the alkyl length of the polyacrylate polymer component. The phase separation modes depend on intermolecular interactions between small molecule TIPSE pentancene and polymer additives. The blend film with a dominant vertical phase separation exhibits a significant enhancement in average mobility and performance consistency of organic thin-film transistors. © *2013 AIP Publishing LLC*. [http://dx.doi.org/10.1063/1.4820588]

Solution-processed organic thin-film transistors (OTFTs) are promising for the next-generation large-area electronics on flexible substrates.[1–3] Semiconducting small molecule/polymer blends, as newly developed, promising active layer systems in OTFTs, take advantages of the high charge-carrier mobility of the semiconducting small molecules, the excellent film formation capability and mechanical properties from polymers, as well as the intriguing phase separation behaviors between the small molecules and polymers.[4,5] Although phase separation behaviors were shown to strongly correlate with charge transport in these systems, no simple and straightforward method to switch between lateral and vertical phase separation modes has been previously reported. Therefore, the exact effect of phase separation modes on crystal alignment and charge transport remains largely underexplored. For example, Hamilton *et al*. blended 6,13-bis(triisopropylsilylethynyl) pentacene (TIPSE pentacene, or TP) or 2,8-difluoro-5,11-bis(triethylsilylethynl)anthradithiophene (diF-TES ADT) with inert and semiconducting polymers, which resulted in improved performance uniformity and simultaneously maintained the peak device performance.[6] Cho and coworkers reported that the vertical phase separation in TES ADT/poly(methylmethacrylate) (PMMA) blends has the potential to an all-solution route to fabricate flexible organic transistors.[7,8] Most recently, Yoon and coworkers explored the phase separation of diF-TES ADT blends with polymers including poly(*alpha*-methylstyrene), PMMA, and syndiotactic polystyrene.[9] A conventional wisdom is that the crystallization of small molecule organic semiconductor dictates the phase separation and self-assembly of polymer-small molecule organic semiconductor blends. However, the effects of specific intermolecular interactions on the phase separation and charge transport of semiconducting small molecule-polymer blends are not well revealed yet.

In this work, we demonstrate the importance of hydrophobic forces in phase separation mode, crystal orientation, as well as charge transport of the small molecule organic semiconductor-polymer blends. We show that by simply varying the length of the hydrophobic side groups in a series of polyacrylate additives, the switching between lateral and vertical phase separations can be easily achieved in solution-crystallized semiconducting small molecule/polymer blend films. Herein, we choose TP[10–12] as a model small molecule to blend with poly(ethyl acrylate) (PEA), poly(butylacrylate) (PBA), and poly(2-ethylhexyl acrylate) (P2EHA), respectively, to demonstrate different phase separation modes. The results show that the vertical phase separation leads to well aligned 2D crystal growth and a large improvement of average mobility and performance consistency.

Figure 1(a) shows the molecule structures of TP and the three polyacrylates: PEA, PBA, and P2EHA. These three polyacrylates have similar weight-average molecular weight and polydispersity index ($M_W$ of 100–120k and PDI of 3), while their hydrophobic side groups differ in the alkyl length: two carbon atoms for PEA, four for PBA, and eight for P2EHA. A simulated molecular view of TP molecules in its needle-shaped crystal is presented in Figure 1(b).[13–15] The red arrow indicates the long axis of the needle shaped TP crystals, and the light blue rods stand for the acene units of TP. Thin films of pristine TP and TP/polymer blends were slowly crystallized in a solvent-rich environment with an optimized weight ratio of 1:1 from dilute toluene solutions (5 mg total solids per ml). The optical micrographs in Figures 1(c)–1(f) show that the pure TP thin film has large crystals with random orientations and poor substrate coverage, while the addition of polyacrylate polymers improves both film coverage and TP crystal alignment at different extents. TP/P2EHA blend film exhibits the most uniform crystal orientation and highest film coverage, while TP/PEA demonstrates the least crystal alignment and coverage enhancement under the same blending and solution crystallization conditions. Therefore, it can be

a)Authors to whom correspondence should be addressed. Electronic addresses: dawenl@eng.ua.edu and chenj1@ornl.gov

 © 2013 AIP Publishing LLC

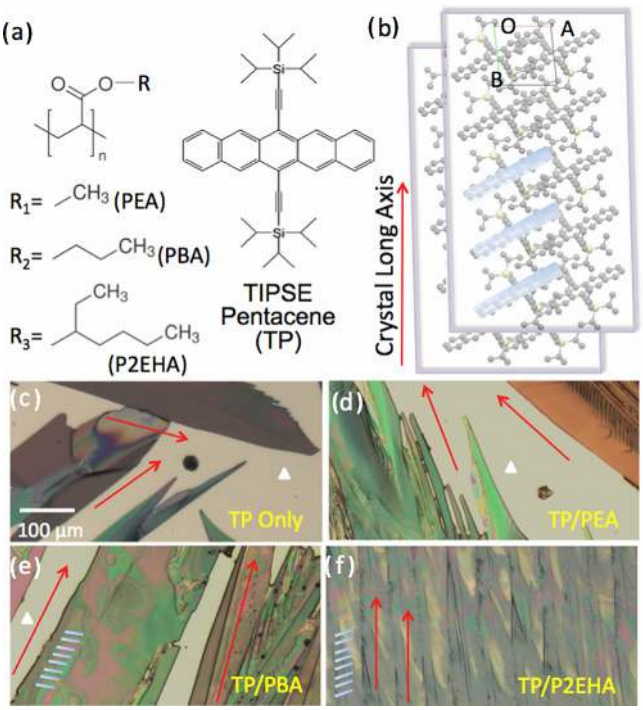


FIG. 1. (a) Molecule structures of TIPSE pentacene, PEA, PBA, and P2EHA. (b) A simulated molecular view of needle-shaped TP crystals on substrate. (c)-(f) Optical micrographs of pure TP film and the three TP/polyacrylate blend films (weight ratio of 1:1). The red arrows in (b)–(f) indicate the long axis of the needle shaped TP crystals, and the tilted light blue rods represent the directions of TP backbones. The triangles mark the uncovered substrate areas. All optical images share the same scale bar of 100 $\mu$m in (c).

inferred that the effect of polyacrylate polymer additives on the TP thin film morphology can be correlated to the length of the polymer hydrophobicity side group.

To examine the influence of crystal alignment on charge transport in the TP/polyacrylate films, bottom-gate, bottom-contact OTFTs were fabricated. Gold electrodes were patterned on heavily doped *n*-type silicon substrate by using standard photolithography followed by metal deposition and lift-off. The silicon substrate with a 100 nm thermal oxide was surface treated with hexamethyldisilazane (HMDS) followed by gold contact treatment using pentafluorobenzenethiol (PFBT).[16,17] HMDS self-assembled monolayer was formed on the gate dielectric by vapor deposition at 140 °C, and rinsing by isopropanol. PFBT treatment on the source/drain contacts was carried out by immersing the substrates in a 10 mM PFBT/toluene solution for 2 h, and rinsing them with toluene. Electrical characterization of OTFTs was carried out in ambient environment at room temperature using an Agilent B1500A semiconductor parameter analyzer. Typical output and transfer characteristics of TP/P2EHA based OTFTs are shown in Figures 2(a) and 2(b). The extracted field-effect mobility and threshold voltage ($V_T$) are 0.33 $cm^2V^{-1}$ $s^{-1}$ and 6 V, respectively, and the on-/off- current ratio obtained from the logarithmic plot of transfer characteristics is $9.6 \times 10^3$. Figure 2(c) clearly shows that the addition of acrylate polymers, in general, reduces mobility variation. The field-effect mobilities of pure TP based OTFTs vary by four orders of magnitude ($2.4 \times 10^{-1}$–$8.3 \times 10^{-4}$ $cm^2 V^{-1} s^{-1}$), while TP/PEA, TP/PBA, and TP/P2EHA based OTFTs demonstrate hole mobilities of 0.04–0.29 $cm^2$ $V^{-1}$ $s^{-1}$, 0.09–0.34 $cm^2$ $V^{-1}$ $s^{-1}$, and 0.26–0.43 $cm^2$ $V^{-1}$ $s^{-1}$, respectively. Figure 2(d) provides a comparison of average mobility (with standard deviation) before and after the addition of acrylate polymers. Average mobility and the associated standard deviation are based on eight measurements for each type of active layer. Pure TP based devices show an average hole mobility of 0.06 $cm^2$ $V^{-1}$ $s^{-1}$, and the addition of PEA, PBA, and P2EHA enhances the average hole mobility to 0.14, 0.16, and 0.35 $cm^2$ $V^{-1}$ $s^{-1}$, respectively. Notably, the addition of P2EHA into TP leads to a six-fold enhancement in average hole mobility as compared to pure TP devices. Furthermore, the ratio of average mobility ($\mu_{Ave}$) to the standard deviation of measured mobility ($\mu_{Stdev}$) is used to represent the performance consistency of OTFTs.[18] The devices based on TP/PEA and TP/PBA blends have $\mu_{Ave}/\mu_{Stdev}$ values increased by 2- and 3-fold, respectively, while TP/P2EHA based devices demonstrated a nine-fold enhancement in performance consistency (or $\mu_{Ave}/\mu_{Stdev}$).

In order to understand the reason of the significantly enhanced crystal alignment and OTFT performance in TP/polyacrylate (especially TP/P2EHA) polymer blend films, energy filtered transmission electron microscopy (EF-TEM) was carried out. A Zeiss Libra 120 at accelerating voltage of 120 kV was used to image the solution-crystallized films in planar view. Each TP/polymer blend was imaged at $0 \pm 5$ eV and $20 \pm 5$ eV, respectively, as shown in Figure 3. The 0 eV (elastic) image reveals features based on electron density contrast, including mass-thickness (composition) contrast and topographical thickness variation. Higher electron density results in darker regions in 0 eV TEM images because of less transmitted electron signals. The 20 eV image specifically highlights the low-eV plasmon contribution from the *p*-type organic semiconductor, in which the brighter areas refer to higher *p*-type TIPSE pentacene semiconductor content.[19,20] Furthermore, thickness maps were generated by taking the intensity ratio of an elastic and unfiltered image, giving a thickness variation based on pixel-by-pixel values of $t/\lambda$, where t is the thickness in nm and $\lambda$ is the mean free pathway of the electron (an unknown constant in this case). The brighter region in a thickness map corresponds to a higher value of $t/\lambda$. In Figure 3, the TP-rich regions are generally darker in elastic (0 eV) image because of the crystallinity of TP and the correspondingly higher electron density, while they are brighter in the 20 eV image because of the low-eV plasmon contribution from TP. The 20 eV image and thickness map nicely decouples the different features in the elastic image, which are evidently caused by both composition contrast and thickness variation. For the TP/P2EHA blend, the featureless appearances in elastic image and thickness map, together with broad edges in 20 eV image imply vertical phase separation and intimate interpenetration between TP- and P2EHA-rich regions. On the other hand, for both TP/PBA and TP/PEA films, sharp crystal edges are often observed. TP/PEA shows identical features between 0 eV, 20 eV image, and thickness map, which agrees with a dominating lateral phase separation mode. In the 20 eV image of TP/PBA film, white circles highlight some of the features (20-50 nm in size) absent in the corresponding elastic image and thickness map, suggesting that there are some

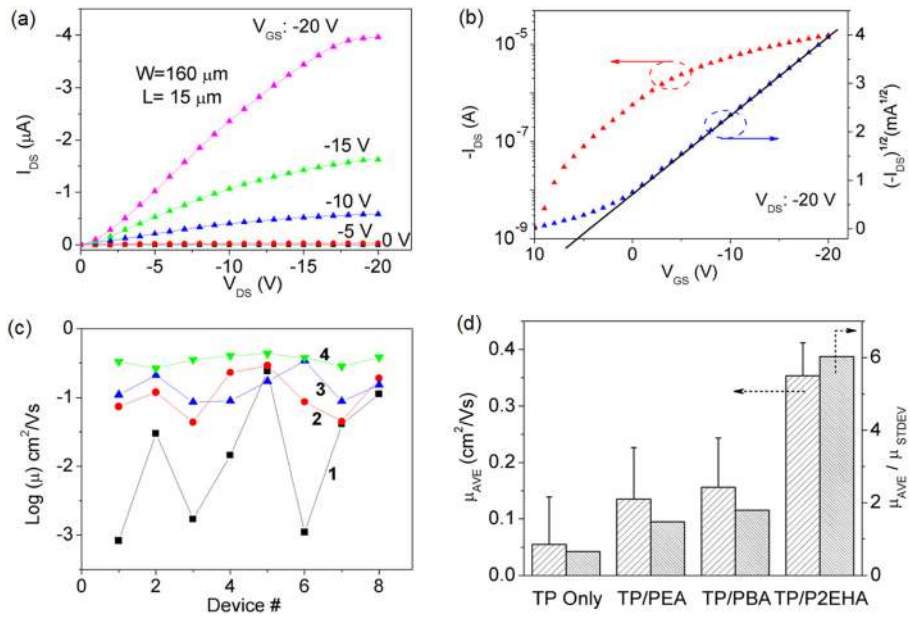


FIG. 2. Typical (a) output and (b) transfer characteristics of TP/P2EHA blend based OTFTs. Curves 1–4 in (c) represent devices based on pure TP, TP/PEA, TP/PBA, and TP/P2EHA, respectively. (d) Comparison of average hole mobility and performance consistency (represented by the value of $\mu_{Ave}/\mu_{Stdev}$).

minor vertical but major lateral phase separations between TP and PBA.

Besides the planar view study by EF-TEM, cross-sectional SEM and contact angle measurements were also conducted to provide additional insight into the nature of phase separation in the TP/polyacrylate systems. Cross-sectional SEM experiments are carried out on cryo-fractured films in a charge compensation mode (i.e., with localized nitrogen flushing). Relatively low accelerating voltage of 1.7 kV is used to minimize charging effect. Samples were immersed in liquid nitrogen, allowed to equilibrate, and cleaved before performing cross-section SEM experiments in a Zeiss Merlin. As shown in cross-sectional SEM view (Figures 4(a) and 4(b)), TP/PBA and TP/P2EHA exhibit monolayer and trilayer structures, respectively. To identify the composition in each structure, static contact angle measurements were performed using a Kruss DSA30 system. The contact angles of deionized water are summarized in Table I. The average contact angle value and standard deviation were estimated based on up to 15 measurements for each film type with sessile fittings. The pure PEA, PBA, and P2EHA surfaces have an average water contact angle of 78.1 ± 1.3°, 102.5 ± 1.5°, and 108.0 ± 1.8°, respectively, showing progressively increasing hydrophobicity as expected. To ensure accuracy and minimize the influence from the substrate, contact angles of pure TP films were measured on both typical TP film (poorly covered) and selected, highly covered area of TP film. The poorly covered TP film has a water contact angle of 84.5 ± 5.6°, while its

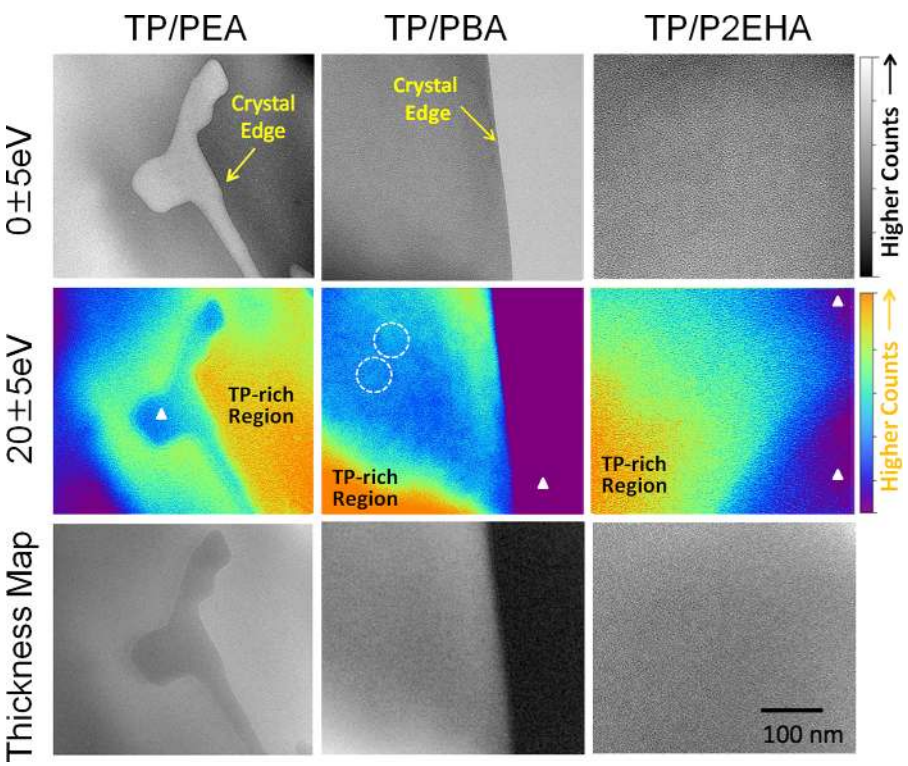


FIG. 3. Energy filtered TEM images (planar view) of TP blends with PEA, PBA, and P2EHA polymer. For each blend, images at 0 ± 5 eV (elastic) and 20 ± 5 eV, and corresponding thickness maps are presented. All images share the same scale bar at bottom right (100 nm). In general, the TP-rich region is darker in elastic image, and brighter in the 20 eV image. TP-deficient regions are marked with white triangles.

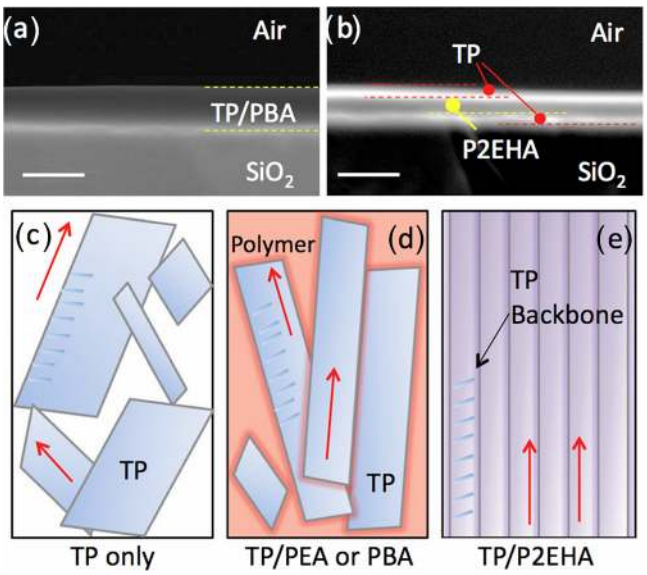


FIG. 4. Cross-sectional SEM images of (a) TP/PBA with a monolayer structure and (b) TP/P2EHA film with a trilayer configuration. The scale bars are 200 nm. (c)–(e) illustrate the effect of phase separation on crystal alignment. TP/PEA film has a dominating lateral phase separation, providing limited crystal confinement. TP/P2EHA demonstrates mainly vertical phase separation, providing excellent 2D confinement for crystal growth. TP/PBA has some minor vertical but mainly major lateral phase separations, providing intermediate crystal alignment. The red arrows stand for the long axis of the needle shaped TP crystals, and the light blue rods represent the TP backbones.

well-covered areas exhibit a contact angle of $99.6 \pm 3.6°$. TP/P2EHA film has a water contact angle of $101.6 \pm 1.6°$, which is reasonably close to the value from well covered TP film ($99.6 \pm 3.6°$). This provides direct evidence that the TP layer is on the top of the observed TP/P2EHA trilayer structure. Considering the top and bottom layers in the cross-sectional SEM (Figure 4(b)) share similar contrast, this leads to the conclusion that both top and bottom layers of the trilayer structure are TP-rich. This proposed trilayer layout of TP/P2EHA film agrees well with the vertical phase separation structure of TP/poly(*alpha*-methylstyrene) film reported in literature.[21] In contrast, the TP/PEA blend film has largely fluctuating water contact angles of $96.9 \pm 11.9°$, further supporting the conclusion that it has a lateral phase separation mode with TP and PEA components side by side. The lower side of the measured contact angles of TP/PEA is likely caused by the relatively small contact angle of PEA ($78.1 \pm 1.3°$), while the higher side results from the higher contact angle of TP ($99.6 \pm 3.6°$ for the well covered regions). The TP/PBA film has an intermediate contact angle fluctuation ($104.7 \pm 3.0°$), which can be attributed to a mixture of lateral and vertical phase separation modes coexists and the fact that TP and PBA have similar water contact angles.

TABLE I. Water contact angle measurements on TP and TP/polymer blend films. The average and standard deviation values are based on up to 15 measurements for each surface.

| | Average (deg) | Standard deviation (deg) |
|---|---|---|
| PEA only | 78.1 | 1.3 |
| PBA only | 102.5 | 1.5 |
| P2EHA only | 108.0 | 1.8 |
| TP only[a] | 99.6 | 3.6 |
| TP only[b] | 84.5 | 5.6 |
| TP/PEA | 96.9 | 11.9 |
| TP/PBA | 104.7 | 3.0 |
| TP/P2EHA | 101.6 | 1.6 |

[a]The selected, well-covered regions of TP film.
[b]The typical, poorly covered regions of TP film.

Finally, the schematic in Figures 4(c)–4(e) is employed to illustrate how the phase separation affects crystal alignment. TP/PEA film has a dominating lateral phase separation, which only leads to limited crystal growth confinement, while TP/PBA film has minor vertical but major lateral phase separation, providing intermediate crystal confinement. TP/P2EHA film, with a confirmed trilayer structure in vertical phase separation mode, provides excellent 2D confinement for TP crystal growth and thus the best OTFT performance.[5]

For a binary blend of solute and solvent, the Gibbs free energy of mixing ($\Delta G$) has the following expression based on Flory-Huggins theory:[22]

$$\frac{\Delta G}{RT} = \sum_{i=1}^{2} n_i \ln \phi_i + n_1 \phi_2 \chi, \tag{1}$$

where $n_i$ is the number of moles for each component, $\phi_i$ is the corresponding volume fraction, and $\chi$ is the interaction parameter between the two components. In Eq. (1), the first term on the right side is the combinatorial entropy change, while the second term is largely considered as contact dissimilarity. Similarly, in a three-component blend system (i.e., TP, polymer, and solvent in our case), the free energy of mixing is expressed as[23]

$$\frac{\Delta G}{RT} = \sum_{i=1}^{3} n_i \ln \phi_i + \Gamma(T, \phi, N), \tag{2}$$

$$\Gamma(T, \phi, N) = n_1 \phi_2 g_{12} + n_1 \phi_3 g_{13} + n_2 \phi_3 g_{23} + n_1 \phi_2 \phi_3 g_{123}, \tag{3}$$

where $\sum_{i=1}^{3} n_i \ln \phi_i$ is the combinatorial entropy term, $\Gamma(T, \phi, N)$ accounts for both non-combinatorial entropy of mixing and enthalpy changes, $g_{ij}$ (i and j = 1, 2, or 3) is the composition-dependent binary interaction parameter, and $g_{123}$ is the ternary interaction parameter. In a polymer containing ternary blend, $\Gamma$ is also a function of the degree of polymerization ($N$).

From a thermodynamic point of view, Eqs. (2) and (3) provide a basis to understand the interplay between the different components in a ternary system (TP, polymer and solvent). It is expected that the long alkyl side chains of P2EHA slightly reduce the effect of the combinatorial entropy ($\sum_{i=1}^{3} n_i \ln \phi_i$) because of their slightly larger size as compared to the side groups of PEA and PBA.[22,23] At the same time, they also contribute to a significantly decreased $\Gamma(T, \phi, N)$ (likely through a large enthalpy change) in TP/P2EHA solution because of their largely increased hydrophobicity, driving the system towards phase separation ($\Delta G < 0$) in the early stage of solvent evaporation to form the top layer of TP. Crystallization plays important kinetic roles in phase separation, which is attributed to the fact that TP forms the top layer. The residual blend solution

consequently has a much-increased P2EHA concentration, favoring the middle layer formation through P2EHA precipitation. Finally, as the rest of the solvent evaporates, the residual TP component forms the bottom layer in Figure 4(b). This vertical phase separation and sequential layer formation resultant from slow solution crystallization of TP/P2EHA effectively confine the highly anisotropic TP crystals into a well-aligned 2D growth pattern. In contrast, the polarity of PEA is expected to correspond to a large $\Gamma(T, \phi, N)$, which contributes to a positive $\Delta G$ and delays the phase separation until the majority of solvent evaporates out. This forces PEA to precipitate with the semiconducting small molecules side-by-side, and only provides limited confinement effect and charge transport enhancement.

In summary, by systematically varying the hydrophobicity (alkyl length) of the polymer additive in a model semiconducting small molecule/polymer blend, switching between the lateral and vertical phase separations is demonstrated. The blend system with vertical phase separation exhibits well-aligned TP crystals, leading to a significant enhancement in average mobility and performance consistency of OTFTs. The results from this work shed light on the important but underexplored interplay among phase separation mode, crystal alignment, and charge transport of solution crystallized, semiconducting small molecule/polymer blends.

Please see supplementary material for X-ray diffraction (XRD) information.[24]

This work was supported by National Science Foundation (NSF ECCS-1151140) and the Center for Materials for Information Technology (MINT) at the University of Alabama. A portion of this research was conducted at the Center for Nanophase Materials Sciences, which is sponsored at Oak Ridge National Laboratory by the Division of Scientific User Facilities, Office of Basic Energy Sciences, and U.S. Department of Energy.

[1]H. Sirringhaus, Adv. Mater. **17**, 2411 (2005).
[2]D. W. Li and L. J. Guo, J. Phys. D: Appl. Phys. **41**, 105115 (2008).
[3]D. W. Li and L. J. Guo, Appl. Phys. Lett. **88**, 063513 (2006).
[4]J. Smith, W. M. Zhang, R. Sougrat, K. Zhao, R. P. Li, D. K. Cha, A. Amassian, M. Heeney, I. McCulloch, and T. D. Anthopoulos, Adv. Mater. **24**, 2441 (2012).
[5]T. Ohe, M. Kuribayashi, R. Yasuda, A. Tsuboi, K. Nomoto, K. Satori, M. Itabashi, and J. Kasahara, Appl. Phys. Lett. **93**, 053303 (2008).
[6]R. Hamilton, J. Smith, S. Ogier, M. Heeney, J. E. Anthony, I. McCulloch, J. Veres, D. D. C. Bradley, and T. D. Anthopoulos, Adv. Mater. **21**, 1166 (2009).
[7]W. H. Lee, D. Kwak, J. E. Anthony, H. S. Lee, H. H. Choi, D. H. Kim, S. G. Lee, and K. Cho, Adv. Funct. Mater. **22**, 267 (2012).
[8]W. H. Lee, J. A. Lim, D. Kwak, J. H. Cho, H. S. Lee, H. H. Choi, and K. Cho, Adv. Mater. **21**, 4243 (2009).
[9]N. Shin, J. Kang, L. J. Richter, V. M. Prabhu, R. J. Kline, D. A. Fischer, D. M. DeLongchamp, M. F. Toney, S. K. Satija, D. J. Gundlach, B. Purushothaman, J. E. Anthony, and D. Y. Yoon, Adv. Funct. Mater. **23**, 366 (2013).
[10]H. J. Jung, Y. J. Shin, Y. J. Park, S. C. Yoon, D. H. Choi, and C. Park, Adv. Funct. Mater. **20**, 2903 (2010).
[11]D. H. Kim, D. Y. Lee, H. S. Lee, W. H. Lee, Y. H. Kim, J. I. Han, and K. Cho, Adv. Mater. **19**, 678 (2007).
[12]I. Bae, S. J. Kang, Y. J. Shin, Y. J. Park, R. H. Kim, F. Mathevet, and C. Park, Adv. Mater. **23**, 3398 (2011).
[13]S. C. B. Mannsfeld, M. L. Tang, and Z. A. Bao, Adv. Mater. **23**, 127 (2011).
[14]Z. R. He, J. H. Chen, Z. Z. Sun, G. Szulczewski, and D. W. Li, Org. Electron. **13**, 1819 (2012).
[15]G. Giri, E. Verploegen, S. C. B. Mannsfeld, S. Atahan-Evrenk, D. H. Kim, S. Y. Lee, H. A. Becerril, A. Aspuru-Guzik, M. F. Toney, and Z. A. Bao, Nature **480**, 504 (2011).
[16]J. A. Lim, W. H. Lee, H. S. Lee, J. H. Lee, Y. D. Park, and K. Cho, Adv. Funct. Mater. **18**, 229 (2008).
[17]B. K. C. Kjellander, W. T. T. Smaal, J. E. Anthony, and G. H. Gelinck, Adv. Mater. **22**, 4612 (2010).
[18]Z. R. He, K. Xiao, W. Durant, D. K. Hensley, J. E. Anthony, K. L. Hong, S. M. Kilbey, J. H. Chen, and D. W. Li, Adv. Funct. Mater. **21**, 3617 (2011).
[19]L. F. Drummy, R. J. Davis, D. L. Moore, M. Durstock, R. A. Vaia, and J. W. P. Hsu, Chem. Mater. **23**, 907 (2011).
[20]J. H. Chen, X. Yu, K. L. Hong, J. M. Messman, D. L. Pickel, K. Xiao, M. D. Dadmun, J. W. Mays, A. J. Rondinone, B. G. Sumpter, and S. M. Kilbey, J. Mater. Chem. **22**, 13013 (2012).
[21]J. Kang, N. Shin, D. Y. Jang, V. M. Prabhu, and D. Y. Yoon, J. Am. Chem. Soc. **130**, 12273 (2008).
[22]P. J. Flory, Discuss. Faraday Soc. **49**, 7 (1970).
[23]C. M. Gomez, E. Verdejo, J. E. Figueruelo, A. Campos, and V. Soria, Polymer **36**, 1487 (1995).
[24]See supplementary material at http://dx.doi.org/10.1063/1.4820588 for X-ray diffraction (XRD) information.